

CONTINUOUS SUBDUCTION OF A LITHOSPHERIC PLATFORM NEAR AN OCEANIC TRENCH

S. V. Solov'ev and V. K. Bulgakov

UDC 536.25

We investigate the convective heat exchange of a lithospheric platform in the zone of subduction during its submergence into the earth's mantle. We consider the effect of the angle of submergence, the velocity of motion of the lithospheric platform over the day surface of the ground, and the coefficient of thermal expansion on the heat exchange, the flow structure, and the submergence depth.

We consider a two-dimensional plane model of continuous subduction of a lithospheric platform near an oceanic trench with allowance for the heat of phase change. The physical formulation of the problem is presented in Fig. 1. A horizontal oceanic platform moves toward a continental one with a constant velocity U_0 , and with the same velocity it submerges into the asthenosphere in the zone of the trench at the angle φ to the day surface of the ground (the day) (most often lithospheric platforms in the zone of subduction submerge at an angle of 45° , although on certain portions of island arcs submergence angles from 30 to 90° have been noted [1]). In turn, the continental platform moves with the velocity U_{con} toward the oceanic one. The day in Fig. 1 is "represented" by the continental and oceanic platforms. In this work we model the process of submergence of a lithospheric platform under a continental one. During the submergence into the mantle the substance of the lithosphere is melted. We investigated the influence of the angle of shove φ , the velocity of motion of the oceanic platform U_0 , heat releases in the lithosphere and in the mantle q_v , and lift forces on the flow pattern and the heat exchange in the earth's mantle near the oceanic trench. A mathematical model of continuous subduction of the lithospheric platform near the oceanic trench that describes convective heat exchange in the earth's mantle in the variables of vortex-stream function-temperature for a stationary case is represented by the following dimensionless equations:

$$\text{Re}^2 \left(\frac{\partial \Psi}{\partial Y} \frac{\partial W}{\partial X} - \frac{\partial \Psi}{\partial X} \frac{\partial W}{\partial Y} \right) = \frac{\eta}{\rho} \text{Re} \Delta W + \text{Gr} \left(\frac{\partial \Theta}{\partial Y} - \frac{\partial \Theta}{\partial X} \right), \quad (1)$$

$$W = - \left[\frac{\partial^2 \Psi}{\partial X^2} + \frac{\partial^2 \Psi}{\partial Y^2} \right], \quad (2)$$

$$\frac{\partial \Psi}{\partial Y} \frac{\partial \Theta}{\partial X} - \frac{\partial \Psi}{\partial X} \frac{\partial \Theta}{\partial Y} = \frac{a}{\text{Pe}} \Delta \Theta + \frac{Q}{\rho C \text{Pe}} \quad (3)$$

with the following boundary conditions:

on the side faces:

$$\partial \Theta / \partial X = 0 \text{ at } X = 0 \text{ and } L_x / L_y;$$

$$\Theta = 1 \text{ at } Y = 0 \text{ and } \Theta = 0 \text{ at } Y = 1;$$

Khabarovsk State Technical University, Khabarovsk, Russia. Translated from *Inzhenerno-Fizicheskii Zhurnal*, Vol. 73, No. 6, pp. 1329-1339, November-December, 2000. Original article submitted February 17, 2000.

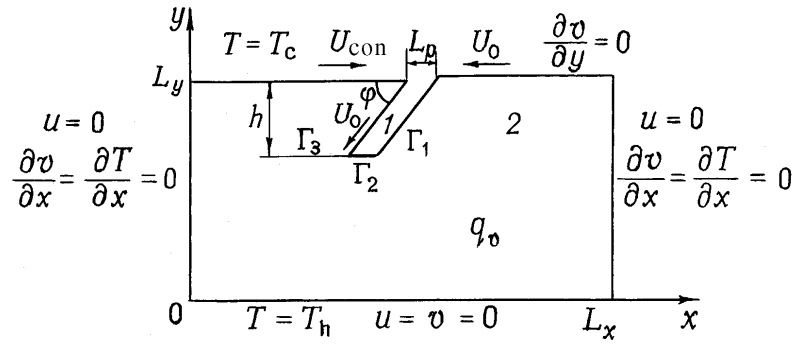


Fig. 1. Physical formulation of the problem: 1) lithosphere; 2) mantle.

on the boundaries Γ_1 and Γ_3 :

$$\frac{\partial \Theta_1}{\partial n} = \frac{\lambda_2}{\lambda_1} \frac{\partial \Theta_2}{\partial n}, \quad \Theta_1 = \Theta_2, \quad \text{where} \quad \frac{\partial \Theta_i}{\partial n} = \frac{\partial \Theta_i}{\partial X} \sin \varphi + \frac{\partial \Theta_i}{\partial Y} \cos \varphi, \quad i = 1, 2;$$

$$\frac{\partial \Psi (0 < X \leq (L_x - L_p)/2L_y, 1)}{\partial Y} = \frac{U_{\text{con}}}{U_o}; \quad \frac{\partial^2 \Psi (0 < X < L_x/L_y, 1)}{\partial X \partial Y} = 0;$$

$$\frac{\partial \Psi ((L_x + L_p)/2L_y \leq X < L_x/L_y, 1)}{\partial Y} = -1; \quad \Psi(0, Y) = \frac{\partial \Psi^2(0, Y)}{\partial X^2} = 0;$$

$$\Psi(L_x/L_y, Y) = \frac{\partial^2 \Psi(L_x/L_y, Y)}{\partial X^2} = 0; \quad \Psi(X, 0) = \frac{\partial \Psi(X, 0)}{\partial Y} = 0;$$

on the boundary Γ_2 :

$$\frac{\partial}{\partial X} \left(\rho \frac{\partial \Psi}{\partial Y} \right) - \frac{\partial}{\partial Y} \left(\rho \frac{\partial \Psi}{\partial X} \right) = 0,$$

$$\frac{\partial \Theta_1}{\partial n} = \frac{\lambda_1}{\lambda_2} \frac{\partial \Theta_2}{\partial n}; \quad \Theta_1 = \Theta_2 = \Theta_{\text{liq}};$$

on the boundaries Γ_1 and Γ_3 and inside the trench:

$$\frac{\partial \Psi}{\partial Y} = -\cos \varphi; \quad \frac{\partial \Psi}{\partial X} = \sin \varphi.$$

To calculate the vortex from Eq. (1) the following boundary conditions were used:

$$W = 0 \text{ at } X = 0, L_x/L_y; \quad W = 0 \text{ at } Y = 0;$$

$$W = - \left[\frac{\partial^2 \Psi}{\partial X^2} + \frac{\partial^2 \Psi}{\partial Y^2} \right] \text{ at } Y = 1.$$

Here the following notation is used: Θ takes the value $\Theta_1 = (T_1 - T_c)/(T_h - T_c)$ for the submerged lithosphere 1 (Fig. 1) and the value $\Theta_2 = (T_2 - T_c)/(T_h - T_c)$ in the earth's mantle 2 (Fig. 1); $X = x/L_y$, $Y = y/L_y$, $\Lambda = \lambda_i/\lambda_2$, $\rho = \rho_i/\rho_2$, $\eta = \mu_i/\mu_2$ ($i = 1, 2$), $Q = q_{vi}L_y^2/\lambda_2(T_h - T_c)$, $W = wL_y/U_o$ and $\Psi = \psi/U_oL_y$;

TABLE 1. Thermophysical Characteristics

Parameters	Lithosphere	Mantle
Viscosity μ , Pa·sec	10^{22}	10^{19}
Thermal conductivity λ , W/(m·K)	3	5
Density ρ , kg/m ³	3000	3300
Specific heat capacity C_p , J/(kg·K)	1200	1200
Coefficient of thermal expansion β , K ⁻¹	$3 \cdot 10^{-5}$	$3 \cdot 10^{-5}$
Heat of melting L_{ph} , J/kg	$4 \cdot 10^5$	$4 \cdot 10^5$
Heat release q_v , W/m ³	$5 \cdot 10^{-6}$	$5 \cdot 10^{-9}$

$$C = \begin{cases} 1, & \Theta < \Theta_s, \\ 1 - \frac{1}{Ste} \frac{\partial \Phi}{\partial \Theta}, & \Theta_s \leq \Theta \leq \Theta_{liq}, \\ 1, & \Theta > \Theta_{liq}, \end{cases} \quad (4)$$

where

$$\frac{\partial \Phi}{\partial \Theta} = \frac{6 (\Theta - \Theta_s) (\Theta - \Theta_{liq})}{(\Theta_{liq} - \Theta_s)^3}.$$

The dimensional value of the dynamic viscosity was determined from the formula

$$\mu = \mu_i (1 + (A - 1)) \left(0.5 + \frac{1}{\pi} \tan \left(\frac{T_s - T_i}{h} \right) \right), \quad i = 1, 2,$$

where $A = [0; 1]$, h is the depth of submergence of the lithospheric platform determined from the melting temperature T_{liq} . The dimensionless dynamic viscosity is calculated from the expression

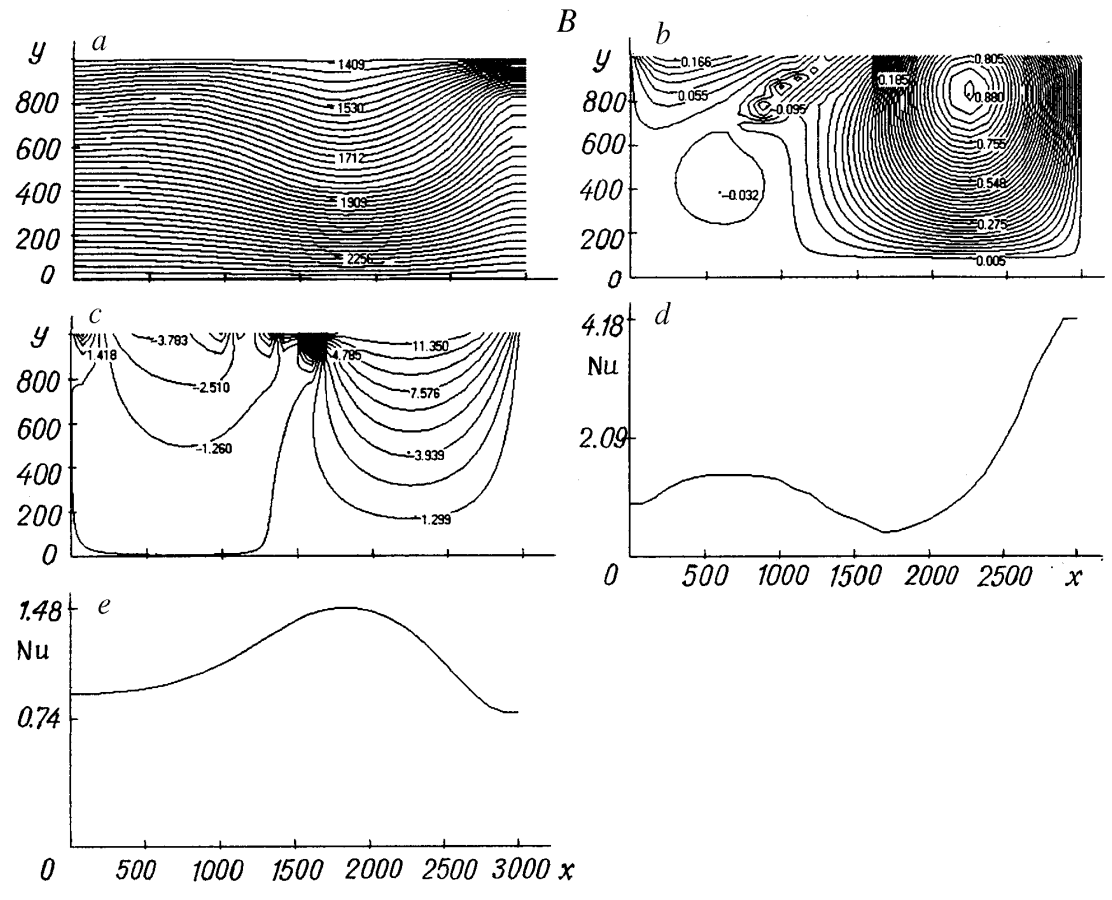
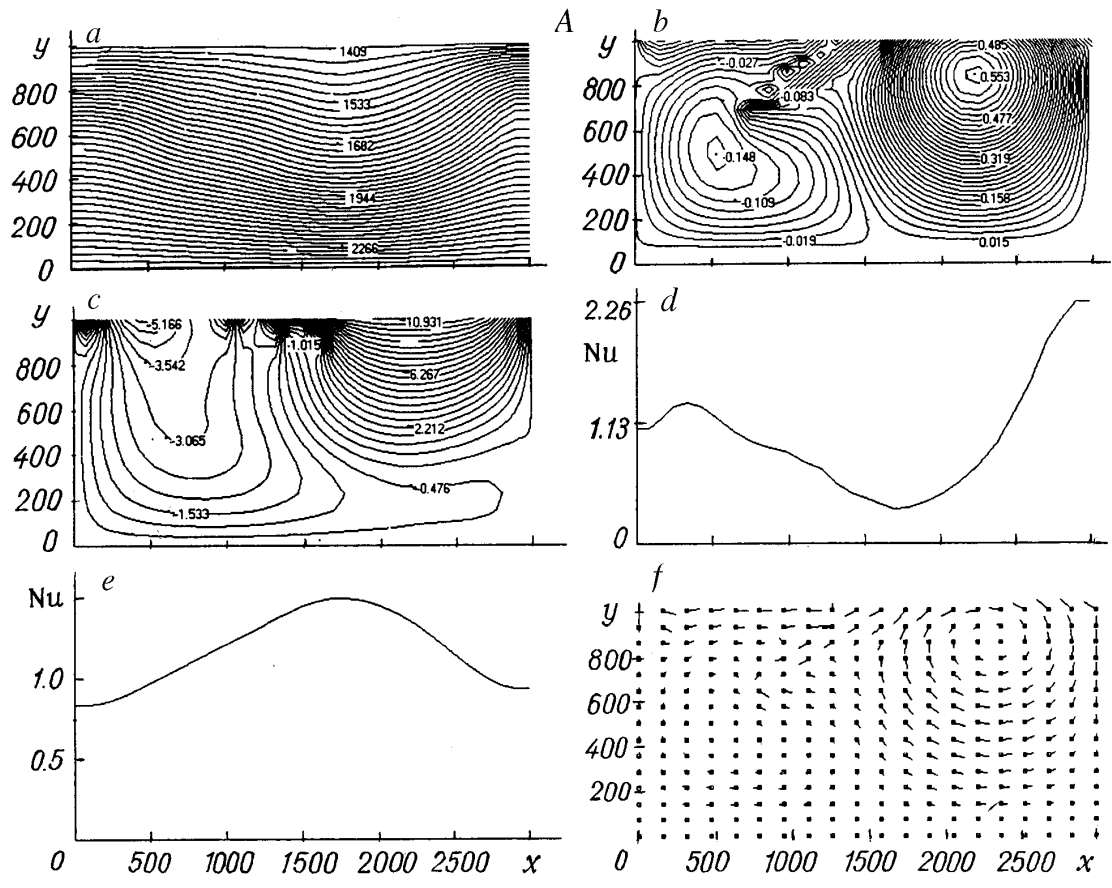
$$\eta = \frac{\mu_i}{\mu_2} (1 + (A - 1)) \left(0.5 + \frac{1}{\pi} \tan \left(\frac{T_s - (T_h - T_c) \Theta_i - T_c}{(1 - Y) H} \right) \right), \quad i = 1, 2, \quad (5)$$

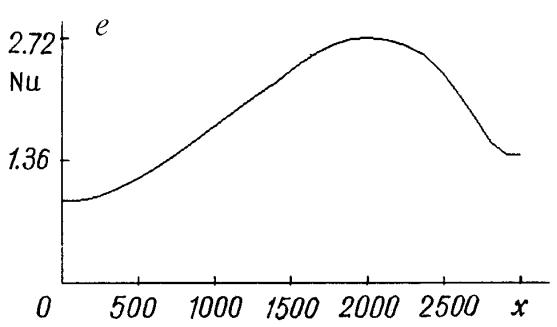
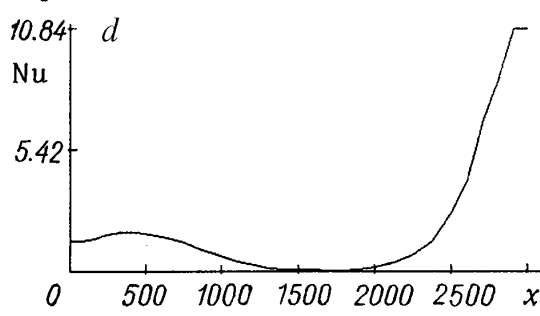
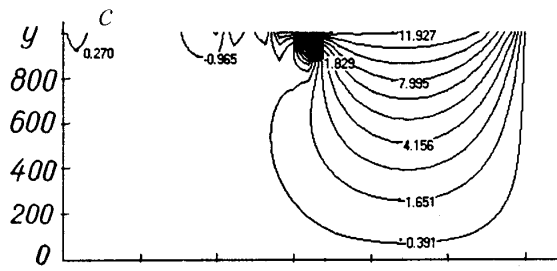
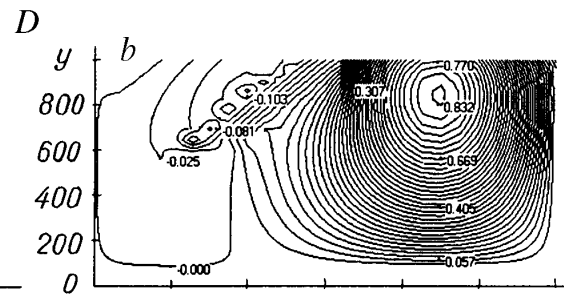
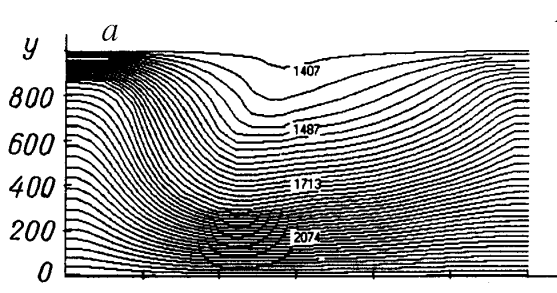
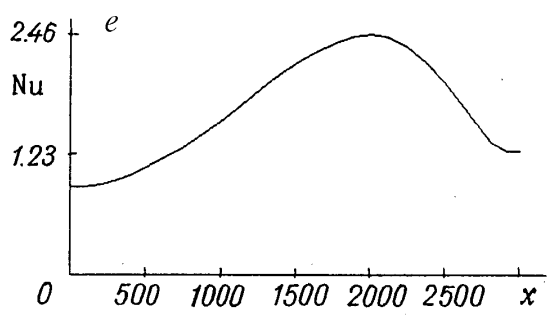
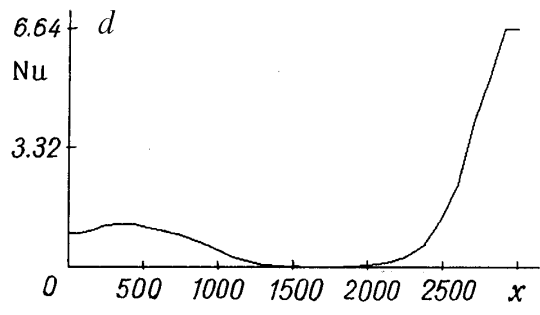
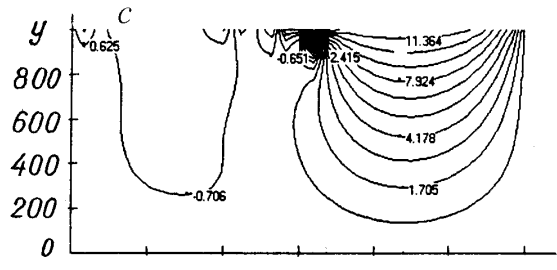
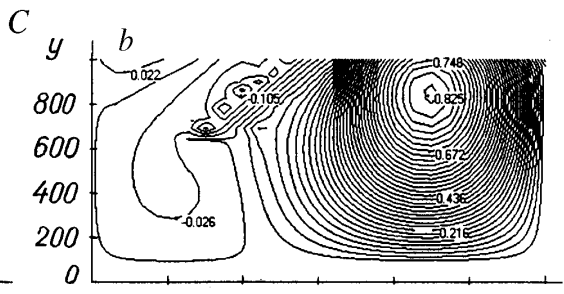
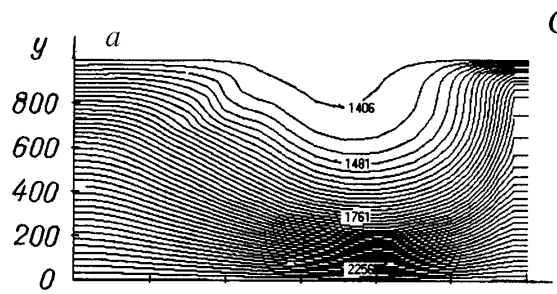
where $H = h/L_y$ is the dimensionless depth of submergence of the lithospheric platform.

The values of the temperature on the upper and lower boundaries of the computational domain are taken to be equal to $T_c = 1400$ K and $T_h = 2400$ K, respectively [1]. The axis of the trench along which the platform submerges is located at the point with the coordinates $(L_x/2, L_y)$, and the thickness (power) of the submerged oceanic platform is equal to L_p . The extension of the computational domain is taken to be equal to 3000 km along the x axis and 1000 km along the y axis. The lower boundary, to which the velocity of submergence of the platform U_o is prescribed and which is known, is determined by the solidus temperature T_s . The problem was solved numerically by the Patankar method [2]. The system of algebraic equations that represents difference analogs of the differential equations (1)-(3) was solved by the Gauss–Zeidel method using lower relaxation.

The dimensionless local Nusselt numbers on the upper ($Y = 1$) and lower ($Y = 0$) boundaries of the computational domain were calculated from the formula

$$Nu|_{Y=1,0} = - \frac{\partial \Theta}{\partial Y} \Big|_{Y=1,0}. \quad (6)$$





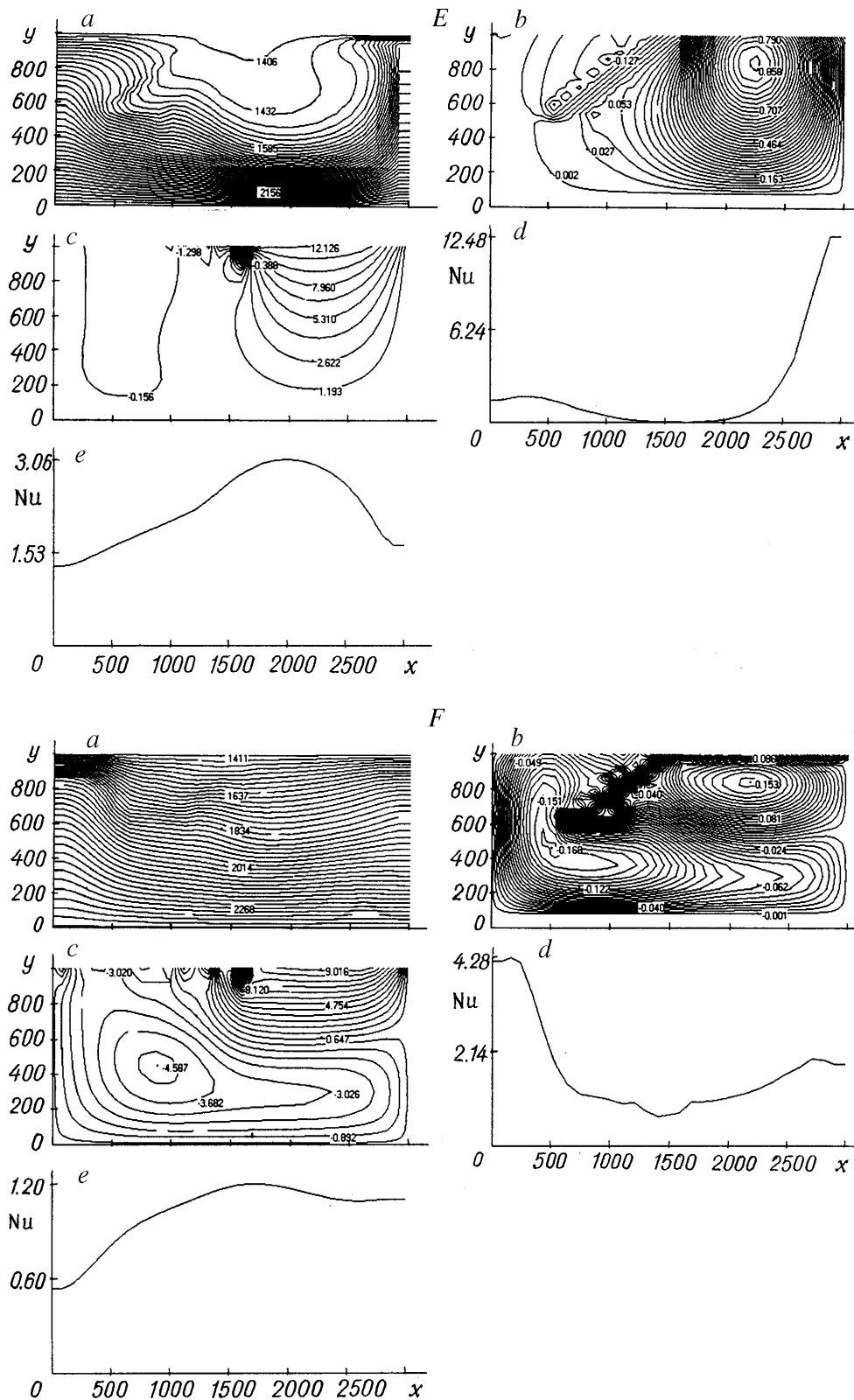


Fig. 2. Computational fields at $\varphi = 30^\circ$: A) $U_0 = 1$ and $\beta = 3 \cdot 10^{-5}$; B) same, without regard for lift forces; C) $U_0 = 3$ and $\beta = 3 \cdot 10^{-5}$; D) $U_0 = 5$ and $\beta = 3 \cdot 10^{-5}$; E) $U_0 = 9$ and $\beta = 3 \cdot 10^{-5}$; F) $U_0 = 3$ and $\beta = 2 \cdot 10^{-4}$ [a) temperature field; b) stream functions; c) vortex; d, e) distribution of the Nusselt numbers on the upper and lower boundaries, respectively; f) vector field of velocity].

As a result of numerical solution of the problem we determined the fields of temperature, stream function, vortex, and velocity and the distribution of the local Nusselt numbers. The values of the dimensional thermophysical quantities used in the calculations are given in Table 1.

In all cases the thickness of the lithosphere L_p was taken to be equal to 100 km. According to data of [1], the temperatures of the solidus T_s and the liquidus T_{liq} were assumed to be 1800 and 1900 K, respectively. The velocity of motion of the continental platform U_{con} was taken to be equal to 1 cm/yr, and the velocity of the oceanic platform U_o was varied within the range 1–9 cm/yr [1].

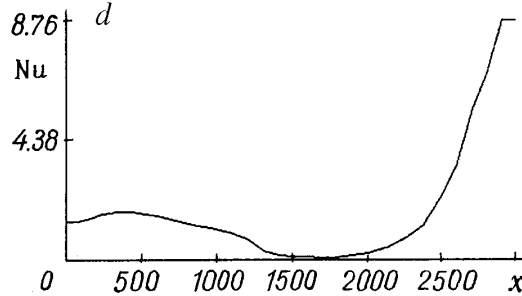
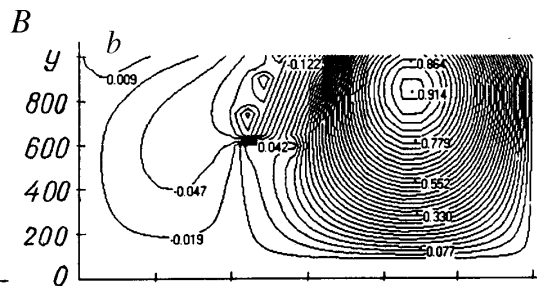
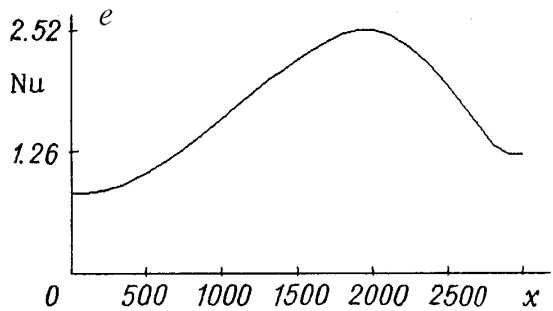
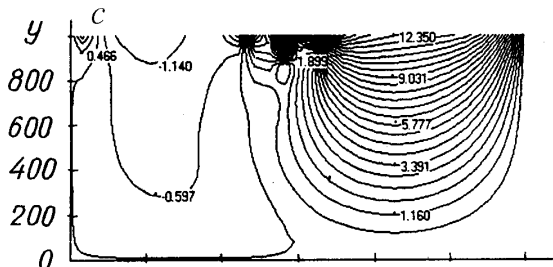
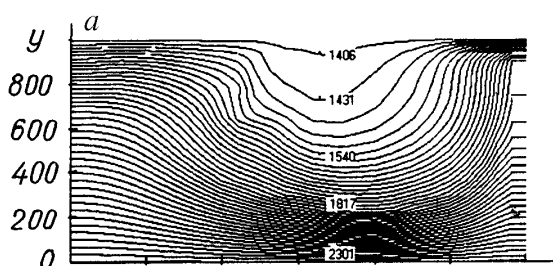
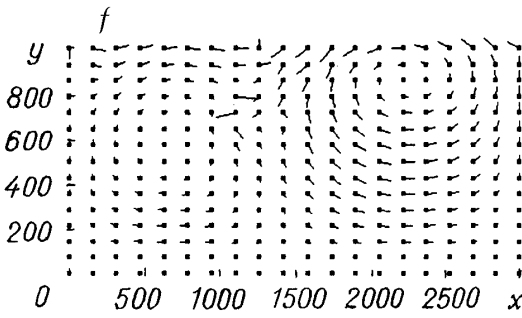
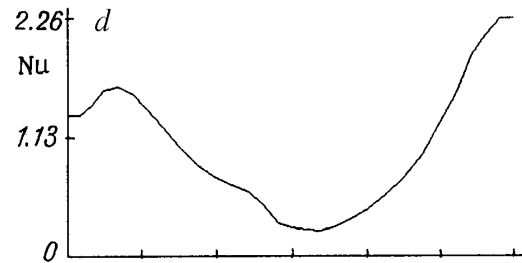
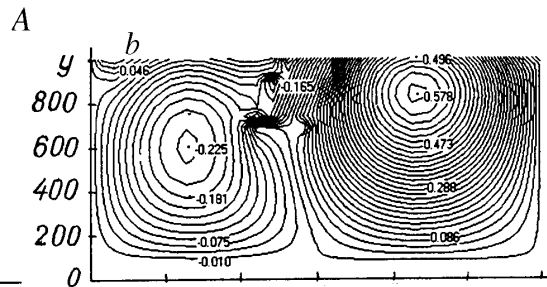
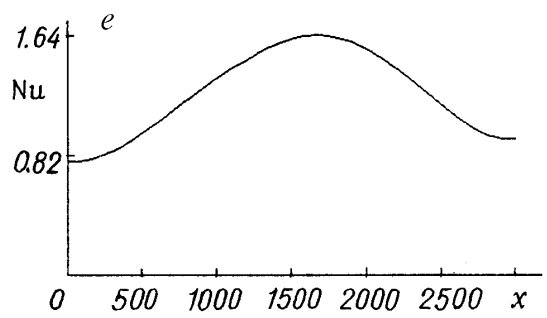
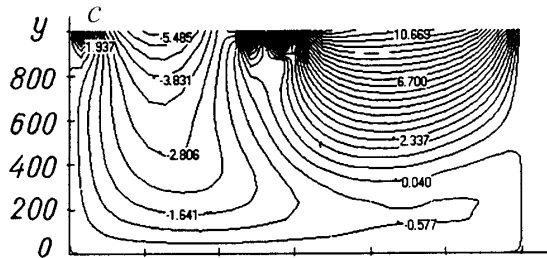
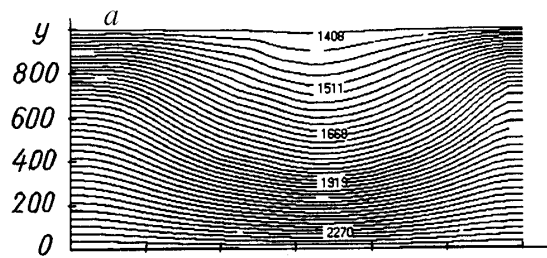
Calculation results for an angle of shove of the lithospheric platform under the continental one $\varphi = 30$ and 60° are presented in Figs. 2 and 3, respectively.

Figure 2A presents calculation results for a velocity of motion of the oceanic platform of 1 cm/yr. The dimensionless similarity numbers had the following values: $Re = 1.05 \cdot 10^{-19}$; $Gr = 3.2 \cdot 10^{-14}$; $Pe = 251$; $Ste = 3$.

We note that for all the variants of calculations considered the Stefan number Ste remained invariable. It is seen from the figure that in the region of the trench the isotherms "bend" downward (Fig. 2A, a); two convective cells form under the oceanic and continental platforms, and they move in opposite directions, with the convective cell and the vortex under the continental platform penetrating into the region of the oceanic convective cell and vortex; this region is located to the right of the zone of subduction (Fig. 2A, b and c). The submerged oceanic platform behaves as if it deforms the continental convective cell by pressing down on it. The depth of submergence of the lithosphere h is equal to about 300 km. Figure 2A, d and e gives the distributions of the Nusselt numbers on the upper and lower boundaries of the computational domain, with the minimum heat flux being noted on the upper boundary (Fig. 2A, d) and the maximum heat flux on the lower boundary (Fig. 2A, e), when $x \sim 1700$ km. It appears that the displacement in the position of the minimum and the maximum of the heat flux from the trench axis ($x = 1500$ km) 200–300 km to the right can be explained by the effect of the convective cell under the continental platform and by its penetration behind the submerged platform. Figure 2B gives results for the same parameters, but without allowance for the lift ($Gr = 0$). Comparing the results of Fig. 2A and Fig. 2B, we can note that the flow pattern changed noticeably, the convective cell under the continental platform decreased considerably (Fig. 2B, b), and the intensity of the vortex increased in the region to the right of the shoved platform and decreased to the left of it (Fig. 2B, c). When the lift forces are not taken into account, heat exchange on the upper boundary of the region increases under the oceanic platform and decreases under the continental one (Fig. 2B, d). On the lower boundary the heat flux virtually did not change (Fig. 2B, e) as compared to the result given in Fig. 2A, e.

As the velocity of motion of the oceanic platform U_o increases to a value of 3 cm/yr (Fig. 2C; $Re = 3.15 \cdot 10^{-19}$; $Pe = 753$), the fields of the temperature, the stream function, and the vortex change in comparison with the results given in Fig. 2A: the oceanic convective cell displaces the continental region located to the left of the trench (Fig. 2C, b). The intensity of the convection of the oceanic cell increases and of the continental cell decreases (Fig. 2A, b and 2C, b). On the upper and lower surfaces of the computational domain heat exchange is intensified, while the minimum of the heat flux on the upper boundary moves toward the trench axis under the influence of the oceanic convective cell (Fig. 2C, d). The depth of submergence of the lithosphere increases to 370 km.

Figure 2D presents results for a velocity of motion of the oceanic platform $U_o = 5$ cm/yr ($Re = 5.25 \cdot 10^{-19}$; $Pe = 1255$). The depth of submergence is equal to a value of the order of 400 km, and the temperature field (Fig. 2D, a) differs noticeably from the result given in Fig. 2C, a. The oceanic convective cell almost completely displaces the continental cell to the region on the left of the trench axis (Fig. 2D, b). In comparison with the results of Fig. 2C, d and e, the heat exchange on the upper boundary increased by a factor of 1.5 (Fig. 2D, d) and virtually did not change on the lower one (Fig. 2D, e). Figure 2E presents results for a velocity of motion of the oceanic platform $U_o = 9$ cm/yr ($Re = 9.45 \cdot 10^{-19}$; $Pe = 2259$). The depth of submergence attains a value of about 500 km. The temperature field changed considerably (Fig. 2E, a) in comparison with the previous result. The intensity of heat exchange continues to increase (Fig. 2E, d and e). The oceanic convective cell occupies practically the entire region (Fig. 2E, b). Figure 2F presents results for $U_o = 3$ cm/yr, but the value of the coefficient of thermal expansion β increased by an order of magnitude, $\beta =$



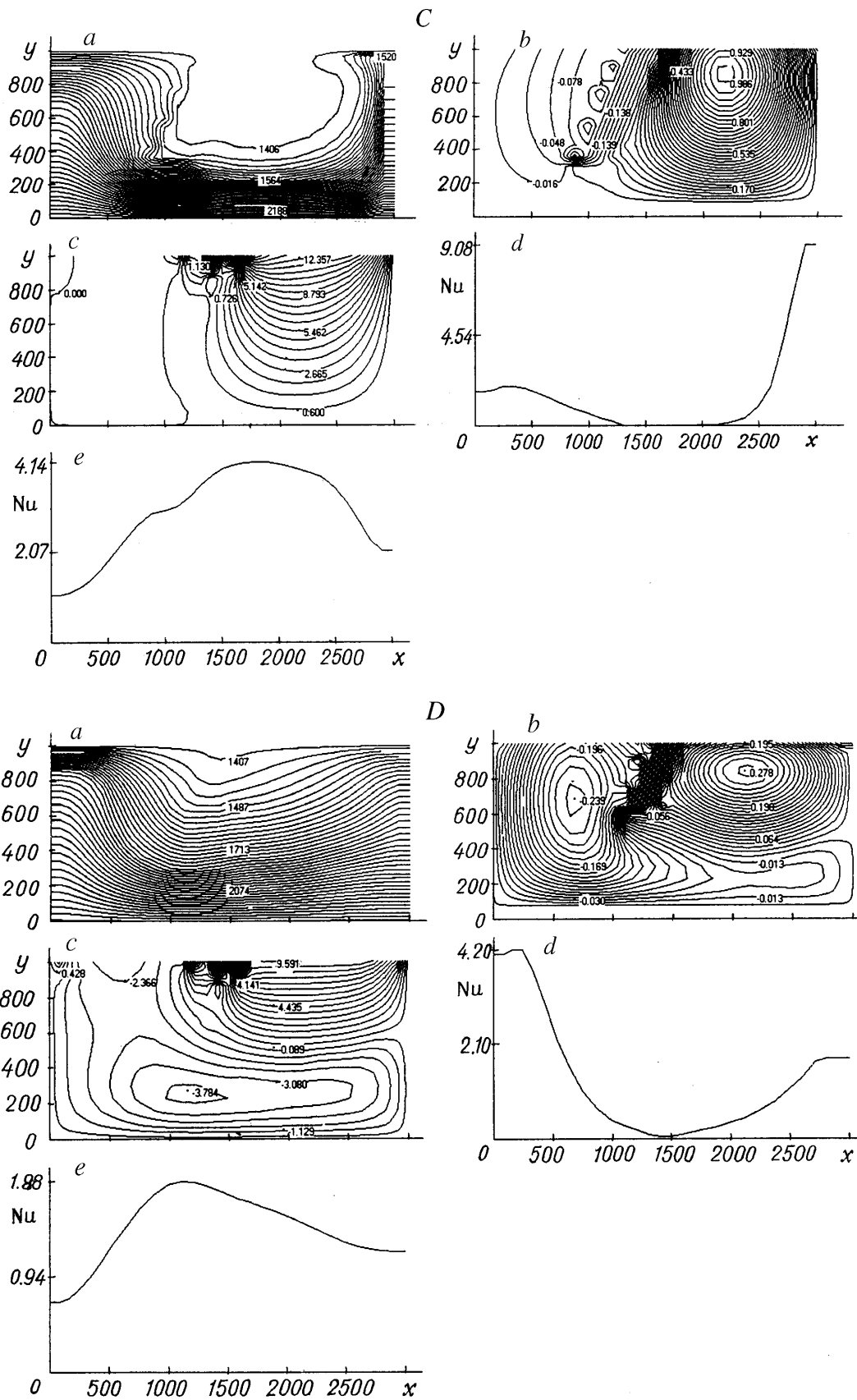


Fig. 3. Computational fields at $\phi = 60^\circ$: A) $U_0 = 1$ and $\beta = 3 \cdot 10^{-5}$; B) $U_0 = 3$ and $\beta = 3 \cdot 10^{-5}$; C) $U_0 = 9$ and $\beta = 3 \cdot 10^{-5}$; D) $U_0 = 3$ and $\beta = 2 \cdot 10^{-4}$ [a-e) the notation is the same as in Fig. 2].

$2 \cdot 10^{-4}$. This increase in β causes the continental convective cell to penetrate into the entire region located behind the submerged platform (Fig. 2F, b). The vertical dimension of the continental convective cell and vortex is equal to about 400 and 600 km, respectively (Fig. 2F, b and c) and of the oceanic ones to 450 and 400 km. The temperature gradients in the region of the trench are less appreciable (Fig. 2F, a) in comparison with the results given in Fig. 2C, c; due to this the intensity of heat exchange on the upper and lower surfaces of the zone of subduction decreases by a factor of 1.5–2 (Fig. 2F, d and e; Fig. 2C, d and e), with a qualitative difference in the character of heat exchange also being present on the upper boundary of the zone of subduction: for the results of Fig. 2F, d heat exchange is enhanced in the region of the left boundary of the zone of subduction ($x < 500$ km) and for the results of Fig. 2C, d in the region of the right boundary ($x > 2500$ km). The maximum of the heat flux on the lower boundary is attained for $x \sim 1700$ km (Fig. 2F, e), while the maximum for the results of Fig. 2C, e is attained for $x \sim 2000$ km.

Figure 3 presents calculation results for an angle of shove $\varphi = 60^\circ$. For $U_o = 1$ cm/yr (Fig. 3A) two large-scale convective cells are formed in the flow region: continental and oceanic ones (Fig. 3A, b). Since the velocity of submergence of the lithosphere is small, the change in the temperature in the region of the trench is insignificant (Fig. 3A, a). The continental vortex penetrates into the region of the oceanic one, pressing it upward (Fig. 3A, c). The fields of the temperature, stream function, and vortex and the distribution of the local Nusselt numbers virtually do not differ (there is only a slight increase in the intensity of convection under the continental and oceanic platforms and heat exchange on the lower boundary) from the corresponding fields for an angle $\varphi = 30^\circ$ (Fig. 2A). Figure 3A, f gives the vector velocity field. An increase in the velocity of the oceanic platform (Fig. 3B; $U_o = 3$ cm/yr) leads to noticeable changes in comparison with the results of Fig. 3A. In the region of the trench the temperature gradients increase, and the temperature field "bends" in the wake of the submerged lithosphere (Fig. 3B, a). The depth of submergence increases from 300 km (Fig. 3A, b) to 400 km (Fig. 3B, b). The oceanic convective cell displaces the continental one beyond the trench axis, the intensities of the oceanic convective cell and vortex increase, and of the continental ones decrease. On the lower and upper boundaries of the region heat exchange is enhanced, and the minimum and the maximum of the heat flux are displaced to the right of the trench axis (Fig. 3A, d and e). For a velocity $U_o = 9$ cm/yr (Fig. 3C) the intensity of convection and heat exchange increases still more appreciably in comparison with the results of Fig. 3B. This is manifested especially strongly in the change in the temperature field (Fig. 3C, a). The depth of submergence of the lithosphere attains a value of the order of 700 km. This exceeds the corresponding values for $\varphi = 30^\circ$ (~ 500 km, Fig. 2E, b). Figure 3D presents calculation results for $U_o = 3$ cm/yr and $\beta = 2 \cdot 10^{-4} \text{ K}^{-1}$ (an order of magnitude larger than for the results presented in Fig. 3A, B, and C). It is seen from the figure that an increase of one order of magnitude in the coefficient of thermal expansion β leads to a change in the field of flow and temperature in comparison with the results of Fig. 3B ($\beta = 3 \cdot 10^{-5} \text{ K}^{-1}$). The heat exchange on the upper boundary decreases (Fig. 3D, d and 3B, d) by practically a factor of 2 and on the lower boundary by a factor of 1.5 (Fig. 3D, e and 3B, e). The continental convective cell and vortex penetrate into the region on the right behind the trench, thus reducing the scale along the vertical of the oceanic convective cell and vortex by about a factor of 1.5 (Fig. 3D, b and c). On the upper boundary of the subduction zone there are differences in the character and intensity of heat exchange similar to that noted above in comparing the results of Fig. 2F, d and Fig. 2C, d. The positions of the minimum and the maximum of the heat flux are displaced to the left of the trench axis by 100 and 400 km, respectively (Fig. 3D, e and d).

For all the variants of calculation with the aid of the obtained values of the stream function we calculated the velocity field in the earth's mantle. Figures 2A, f and 3A, f present, as an example, vector fields of velocity for shove angles $\varphi = 30$ and 60° . As is seen from these figures, for these values of the shove angle an intense vortex is formed under the oceanic platform and a weak one under the continental platform. The vector velocity fields presented make it possible to track the flow pattern in the earth's mantle.

Thus, as a result of the mathematical simulation of the process of submergence of the lithospheric platform in the zone of subduction and the analysis of the data obtained, the following conclusions can be drawn:

1) for the shove angles considered, with a velocity of the oceanic platform U_o equal to the velocity of the continental platform $U_{con} = 1$ cm/yr, two large-scale continental and oceanic convective cells are formed, with the continental platform penetrating into the region of the oceanic one;

2) with increase in the velocity of motion of the oceanic platform the continental convective cell becomes very small-scale;

3) the depth of submergence of the lithospheric platform depends on the velocity of motion of the oceanic platform and the shove angle;

4) disregard of the lift forces and an increase in the coefficient of thermal expansion lead to considerable changes in the structure of convective cells in the earth's mantle.

NOTATION

L_x and L_y , characteristic linear scales along the x and y axes; U_o and U_{con} , velocities of motion of the oceanic and continental platforms; X , Y , Θ , Λ , ρ , $\eta = \mu_i/\mu_2$ ($i = 1, 2$), Q , W , Ψ , and C , dimensionless coordinates, temperature, thermal-conductivity coefficient, density, dynamic viscosity, internal heat source, stress of the vortex, stream function, and heat capacity, respectively; q_{vi} , dimensional volume density of heat releases in the lithosphere ($i = 1$) and the earth's mantle ($i = 2$); C_p , heat capacity of the lithosphere and the mantle; $a = \Lambda/(\rho C)$, dimensionless coefficient of thermal diffusivity; $a_2 = \lambda_2/(f_2 C_p)$, dimensional coefficient of thermal diffusivity of the mantle substance; L_{ph} , heat of phase change; $\Theta_s = (T_s - T_c)/(T_h - T_c)$ and $\Theta_{liq} = (T_{liq} - T_c)/(T_h - T_c)$, dimensionless solidus and liquidus temperatures; T_1 and T_2 , dimensional running temperatures of the lithosphere and the mantle; T_c and T_h , dimensional temperatures on the upper and lower boundaries of the region, respectively; $Ste = C_p(T_h - T_c)/L_{ph}$, $Re = \rho_2 L_y U_o/\mu_2$, $Gr = \rho_2^2 g \beta (T_h - T_c) L_y^3/\mu_2^2$, and $Pe = U_o L_y/a_2$, dimensionless Stefan, Reynolds, Grashof, and Péclet numbers. Subscripts: o, oceanic; con, continental; 1, characteristics of the lithosphere; 2, characteristics of the mantle; v, volume; ph, phase; p , pressure; s, solid; liq, liquid; c, cold; h, hot.

REFERENCES

1. V. N. Zharkov, *Internal Structure of the Earth and Planets* [in Russian], Moscow (1983).
2. S. Patankar, *Numerical Methods of Solution of Problems of Heat Exchange and Liquid Dynamics* [Russian translation], Moscow (1984).